

Metadensity Functional Theory for Classical Fluids: Extracting the Pair PotentialStefanie M. Kampa¹, Florian Sammüller¹, Matthias Schmidt¹, and Robert Evans²¹*Theoretische Physik II, Physikalisches Institut, Universität Bayreuth, D-95447 Bayreuth, Germany*
²*H. H. Wills Physics Laboratory, University of Bristol, Royal Fort, Bristol BS8 1TL, United Kingdom*

(Received 11 November 2024; accepted 4 February 2025; published 11 March 2025)

The excess free energy functional of classical density functional theory depends upon the type of fluid model, specifically on the choice of (pair) potential. This functional is unknown in general and is approximated reliably only in special cases. We present a machine learning scheme for training a neural network that acts as a generic metadensity functional for truncated but otherwise arbitrary pair potentials. Automatic differentiation and neural functional calculus then yield, for one-dimensional fluids, accurate predictions for inhomogeneous states and immediate access to the pair distribution function. The approach provides a means of addressing a fundamental problem in the physics of liquids and for soft matter design: “How do we best invert structural data to obtain the pair potential?”

DOI: 10.1103/PhysRevLett.134.107301

Classical density functional theory (DFT) is a powerful framework for investigating the equilibrium structure and thermodynamics of bulk and spatially inhomogeneous liquids and more general soft matter systems [1–5]. Rosenfeld’s fundamental measure theory for hard spheres proved pivotal to the field, due to its high accuracy and its beautiful and intriguing geometrical structure [6–9]. The treatment of longer-ranged interparticle attraction, acting on top of short-ranged repulsion, is typically based on a simple additive mean-field contribution to the (accurate) hard sphere free energy density functional [2,3]. Despite its status as a workhorse of DFT, the predictions of the “standard mean-field approach” rarely allow for direct quantitative comparison to simulation results.

To overcome limitations of classical DFT approximations, a range of recent studies addressed the possibility to apply machine learning techniques [10–20]. The neural functional theory [21–28] based on representing the one-body direct correlation functional—the first derivative of the excess free energy functional—by a neural network has proved very successful. The approach allows for extensive use of functional integration and differentiation techniques [21–28] using automatic differentiation [29,30]. Neural functionals were trained for specific interparticle interaction potentials, including three-dimensional hard spheres [21], one-dimensional hard [22] and attractive rods [24,25], three-dimensional supercritical [21,26,27] and subcritical [27] Lennard-Jones (LJ) fluids, and ionic fluids [28].

At the core of these successful machine learning applications [21–28] lie the formally exact functional relationships of DFT [1]. In particular, the density profile $\rho(\mathbf{r})$ determines the one-body direct correlation function $c_1(\mathbf{r})$. Of course, the interparticle interactions and the state point need to be known. For model fluids where particles interact solely with a pair potential $\phi(r)$, with r denoting the interparticle distance, Henderson’s theorem [31] states that knowledge of the pair distribution function $g(r)$ at a single state point is sufficient to determine the pair potential $\phi(r)$ up to a constant. While being a foundational problem [32–36], much current research is devoted to exploring the practicalities and consequences, e.g., for reverse Monte Carlo [35,37], variational methods [38,39], machine learning [26,40,41], sensitivity [42,43], design tasks [44,45], quasiuniversality [46], and microscopy in colloidal systems [47].

Here we demonstrate the feasibility of neural functional training based on local learning of the simultaneous functional dependences on both the density profile $\rho(\mathbf{r})$ and on the thermally scaled pair potential $\beta\phi(r)$, where $\beta = 1/(k_B T)$, with the Boltzmann constant k_B and temperature T . The increase in demand of training data generated from simulations of spatially inhomogeneous systems with varying pair potentials is only very moderate, given the significant increase both in functional complexity and applicability to the general form of $\phi(r)$ and the free choice of the temperature T . As the functional dependence on $\phi(r)$ is often merely treated implicitly, we refer to explicit and accurate functionals of both density and pair potential as metadensity functionals. We apply and test the framework for general one-dimensional interacting fluid models after first describing the underlying theoretical structure.

Published by the American Physical Society under the terms of the Creative Commons Attribution 4.0 International license. Further distribution of this work must maintain attribution to the author(s) and the published article’s title, journal citation, and DOI.

We consider systems of N particles with identical mass m , position coordinates \mathbf{r}_i , and momenta \mathbf{p}_i , where the index i labels the particles with $i = 1, \dots, N$. The Hamiltonian H is taken to consist of a sum of an intrinsic and an external contribution $H = H_{\text{int}} + \sum_{i=1}^N V_{\text{ext}}(\mathbf{r}_i)$, where $V_{\text{ext}}(\mathbf{r})$ is an external potential that acts at (generic) position \mathbf{r} . The intrinsic part H_{int} of the Hamiltonian is the sum of kinetic and interparticle interaction energy, which we restrict to pair contributions only, such that

$$H_{\text{int}} = \sum_{i=1}^N \frac{\mathbf{p}_i^2}{2m} + \frac{1}{2} \sum_{i=1}^N \sum_{j=1, j \neq i}^N \phi(|\mathbf{r}_i - \mathbf{r}_j|), \quad (1)$$

and we comment on more general forms of interparticle potentials $u(\mathbf{r}_1, \dots, \mathbf{r}_N)$ below.

The definition of the intrinsic free energy functional can be based on Levy's constrained search [48,49] or on the standard Mermin argument [1,3,50]. The intrinsic free energy functional consists of an ideal and an excess part according to

$$F[\rho, \beta\phi] = F_{\text{id}}[\rho] + F_{\text{exc}}[\rho, \beta\phi], \quad (2)$$

where $\beta F_{\text{id}}[\rho] = \int d\mathbf{r} \rho(\mathbf{r}) \{\ln[\rho(\mathbf{r})\Lambda^d] - 1\}$ with dimensionality d and thermal de Broglie wavelength Λ ; for convenience, we set $\Lambda = 1$ in the following. The excess free energy functional $F_{\text{exc}}[\rho, \beta\phi]$ accounts for the effects of the interparticle interactions via its functional dependence on $\beta\phi(r)$. Thermal scaling incorporates fully the dependence on temperature T , such that there remains no hidden temperature dependence in $\beta F[\rho, \beta\phi]$, as follows, e.g., from the definition via the Levy search $\beta F[\rho, \beta\phi] = \min_{f \rightarrow \rho} \text{Tr} f(\beta H_{\text{int}} + \ln f)$, where Tr denotes the grand canonical trace, and f the many-body trial distribution function [48,49]. The one-body direct correlation functional follows via functional differentiation [1–5]:

$$c_1(\mathbf{r}; [\rho, \beta\phi]) = -\frac{\delta \beta F_{\text{exc}}[\rho, \beta\phi]}{\delta \rho(\mathbf{r})}. \quad (3)$$

We aim to transcend existing neural functional methods [21–23,26–28] and base our supervised local machine learning on simulation data not only generated by varying the form of the external potential $V_{\text{ext}}(\mathbf{r})$, but also by varying the pair potential $\phi(r)$. For any given training system [given $\phi(r)$], sampling in grand canonical Monte Carlo simulations yields the equilibrium density profile $\rho(\mathbf{r})$ at prescribed T and chemical potential μ . The resulting form of the one-body direct correlation function intended to serve as a reference for the neural training then follows as

$$c_1^{\text{ref}}(\mathbf{r}) = \ln \rho(\mathbf{r}) + \beta V_{\text{ext}}(\mathbf{r}) - \beta \mu. \quad (4)$$

Note that each term on the right-hand side is known, as was exploited in previous work [21–28], and that Eq. (4) is valid for all interparticle potentials.

This data acquisition process is repeated several thousand times for different randomized forms of the scaled external potential $\beta V_{\text{ext}}(\mathbf{r})$, randomized values of the scaled chemical potential $\beta \mu$, and, crucially, also randomized forms of the scaled pair potential $\beta \phi(r)$. Apart from the last ingredient, the training follows that in Refs. [21–23,26–28]. Now we have training data for the construction of the neural metadensity functional $c_1(\mathbf{r}; [\rho, \beta\phi])$, which depends on both the density profile $\rho(\mathbf{r})$ and on the form of the scaled pair interaction potential $\beta \phi(r)$. Specifically, the training aims to achieve equality across the entire training dataset:

$$c_1(\mathbf{r}; [\rho, \beta\phi]) = c_1^{\text{ref}}(\mathbf{r}), \quad (5)$$

where the left-hand side indicates the neural network output and the right-hand side the training reference (4). We represent $c_1(\mathbf{r}; [\rho, \beta\phi])$ by a simple multilayer perceptron with five hidden layers; see Fig. 1 for an illustration in

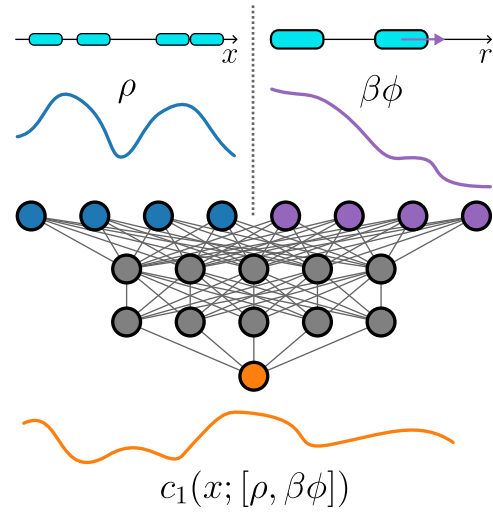


FIG. 1. Training strategy of the neural metadensity functional. Grand canonical Monte Carlo simulations yield training data for supervised machine learning. The simulations are carried out with randomized scaled external potentials $\beta V_{\text{ext}}(x)$ and randomized scaled chemical potentials $\beta \mu$. Results for the density profiles $\rho(x)$ are obtained for randomized scaled interparticle potentials $\beta \phi(r)$. These datasets are used to train a neural one-body direct correlation metadensity functional $c_1(x; [\rho, \beta\phi])$ that renders the simultaneous functional dependence on both fields $\rho(x)$ and $\beta \phi(r)$ operational. Here, x is the one-dimensional position coordinate and r is the interparticle distance. We have used 12 089 simulation runs and truncated $\rho(x)$ symmetrically around each grid point at $\pm 2\sigma$. We restrict ourselves to $\beta \phi(r)$ that vanish beyond the length $r_c = 1.5\sigma$ of its input grid, where σ is the length scale and 0.01σ is the grid spacing [51].

one-dimensional geometry and Refs. [18,26] for possible further architectures.

Ready access to $c_1(\mathbf{r}, [\rho, \beta\phi])$ allows one to obtain the excess free energy functional via functional line integration $-\beta F_{\text{exc}}[\rho, \beta\phi] = \int \mathcal{D}[\rho] c_1(\mathbf{r}; [\rho, \beta\phi])$. In practice, a parametrization with simple scaling $a\rho(\mathbf{r})$ by a parameter $0 \leq a \leq 1$ allows one to numerically integrate according to $-\beta F_{\text{exc}}[\rho, \beta\phi] = \int d\mathbf{r} \rho(\mathbf{r}) \int_0^1 da c_1(\mathbf{r}; [a\rho, \beta\phi])$. The required equilibrium density profile $\rho(\mathbf{r})$ is obtained from a self-consistent solution of the standard Euler-Lagrange equation of DFT [1–5], as follows formally from combining Eqs. (4) and (5): $c_1(\mathbf{r}; [\rho, \beta\phi]) = \ln \rho(\mathbf{r}) + \beta V_{\text{ext}}(\mathbf{r}) - \beta\mu$, where we have kept the functional dependence on the scaled pair potential $\beta\phi(r)$ explicit in the notation. Exponentiating and rearranging yields

$$\rho(\mathbf{r}) = \exp\{c_1(\mathbf{r}; [\rho, \beta\phi]) - \beta V_{\text{ext}}(\mathbf{r}) + \beta\mu\}, \quad (6)$$

which suits the application of iterative solution methods.

We specialize first to bulk fluids where $V_{\text{ext}}(\mathbf{r}) = 0$ and where we expect a spatially homogeneous bulk fluid with constant density $\rho(\mathbf{r}) = \rho_b = \text{const}$. The one-body direct correlation functional is then independent of position \mathbf{r} and directly related to the excess chemical potential μ_{exc} :

$$c_1(\mathbf{r}; [\rho_b, \beta\phi]) = -\beta\mu_{\text{exc}} = \ln \rho_b - \beta\mu, \quad (7)$$

which follows directly from Eq. (6).

Percus test particle limit [52] allows one to access the bulk pair structure. The external potential is chosen to be identical to the pair potential of the fluid $V_{\text{ext}}(\mathbf{r}) = \phi(r)$. The corresponding test particle density profile is $\rho(\mathbf{r}) = \rho_b g(r)$, where $g(r)$ is the standard pair distribution function [3,52]. The general Euler-Lagrange equation (6) then attains test particle form,

$$\rho_b g(r) = \exp\{c_1(r; [\rho_b g, \beta\phi]) - \beta\phi(r) + \beta\mu\}, \quad (8)$$

which applies to any form of $\phi(r)$.

We describe the results for four very different one-dimensional fluids; see Fig. 2, second row. Note that r is then replaced by x in Eq. (8). The models are representative: hard rods [22,53,54], square-shoulder particles [55], random penetrable repulsive particles, and LJ particles.

Predicting pair structure: $g(r)$ —We first take the Hamiltonian (1) to be known. The given $\phi(r)$ can then be used explicitly in the test particle equation (8). A self-consistent solution is efficiently obtained for given values of β, μ via Picard iteration, which delivers results directly for the pair distribution function $g(r)$. This density functional setup of Percus test particle limit applies to any $\phi(r)$ using the same universal metadensity functional $c_1(\mathbf{r}; [\rho, \beta\phi])$, as is demonstrated in Fig. 2 for the four

one-dimensional model fluids. Note the pronounced effect of interparticle attraction (fourth column) on the degree of structuring in $g(r)$. The neural equation of state $\rho_b(\mu)$ follows from Eq. (7); see insets in Fig. 2. The results are numerically identical to reference data obtained from grand canonical Monte Carlo simulations and, for hard rods, to the exact solution [53,56] $\beta\mu_{\text{exc}} = -\ln(1 - \eta) + \eta/(1 - \eta)$ with $\eta = \rho_b \sigma$.

Henderson inversion yields pair potential $\phi(r)$ —Second, we consider the situation where $g(r)$ is known. We take ρ_b, β as the control parameters and obtain μ from Eq. (7). The task is to find $\phi(r)$ that generates this given $g(r)$, which constitutes Henderson’s inversion problem [31]; see Refs. [18,26,32–47]. We render the formal inversion operational by taking the logarithm of Eq. (8) and solving for the explicit occurrence of the pair potential:

$$\beta\phi(r) = c_1(r; [\rho_b g, \beta\phi]) + \beta\mu - \ln[\rho_b g(r)]. \quad (9)$$

Equation (9) constitutes a self-consistency relation for determining $\phi(r)$. Using Picard iteration, we obtain remarkably consistent results, as demonstrated in Fig. 2. On the scale of the figure it is hardly possible to find differences from the (original) pair potential.

Inhomogeneous metadensity functional application—Our method is designed for general density functional setups, where an external potential $V_{\text{ext}}(\mathbf{r})$ is specified, and one aims to calculate the emerging inhomogeneous density profile $\rho(\mathbf{r})$ for a given model fluid. This implies the standard solution of the Euler-Lagrange equation (6), keeping $\phi(r)$ fixed. Figure 3 illustrates the application of this strategy to confinement between two hard walls; this situation was not part of the training set. Note the highly structured density profiles for the LJ fluid in the fourth column. We emphasize that the four fluid models are mere representative examples and that all results stem from the same neural metadensity functional $c_1(\mathbf{r}, [\rho, \beta\phi])$. In situations where the full functional dependence is not required, one can work with parametric dependence on pair potential parameters; see Appendix A for an application to square-shoulder particles and for a discussion of many-body interparticle potentials.

Soft matter inverse design—The flexible dependence on the pair potential inherent in Eq. (6) allows one to go beyond standard density functional tasks and address design problems, similar to Henderson inversion. We hence set the target as the inhomogeneous one-body density profile. This introduces the following intriguing problem: Suppose we have prescribed forms of both $V_{\text{ext}}(\mathbf{r})$ and of $\rho(\mathbf{r})$, at given μ, β . How do we find the specific pair potential $\phi(r)$ that realizes the target, assuming the interparticle potential is described solely by two-body contributions? To accomplish this task, we use Newton’s method to solve the Euler-Lagrange equation (6)

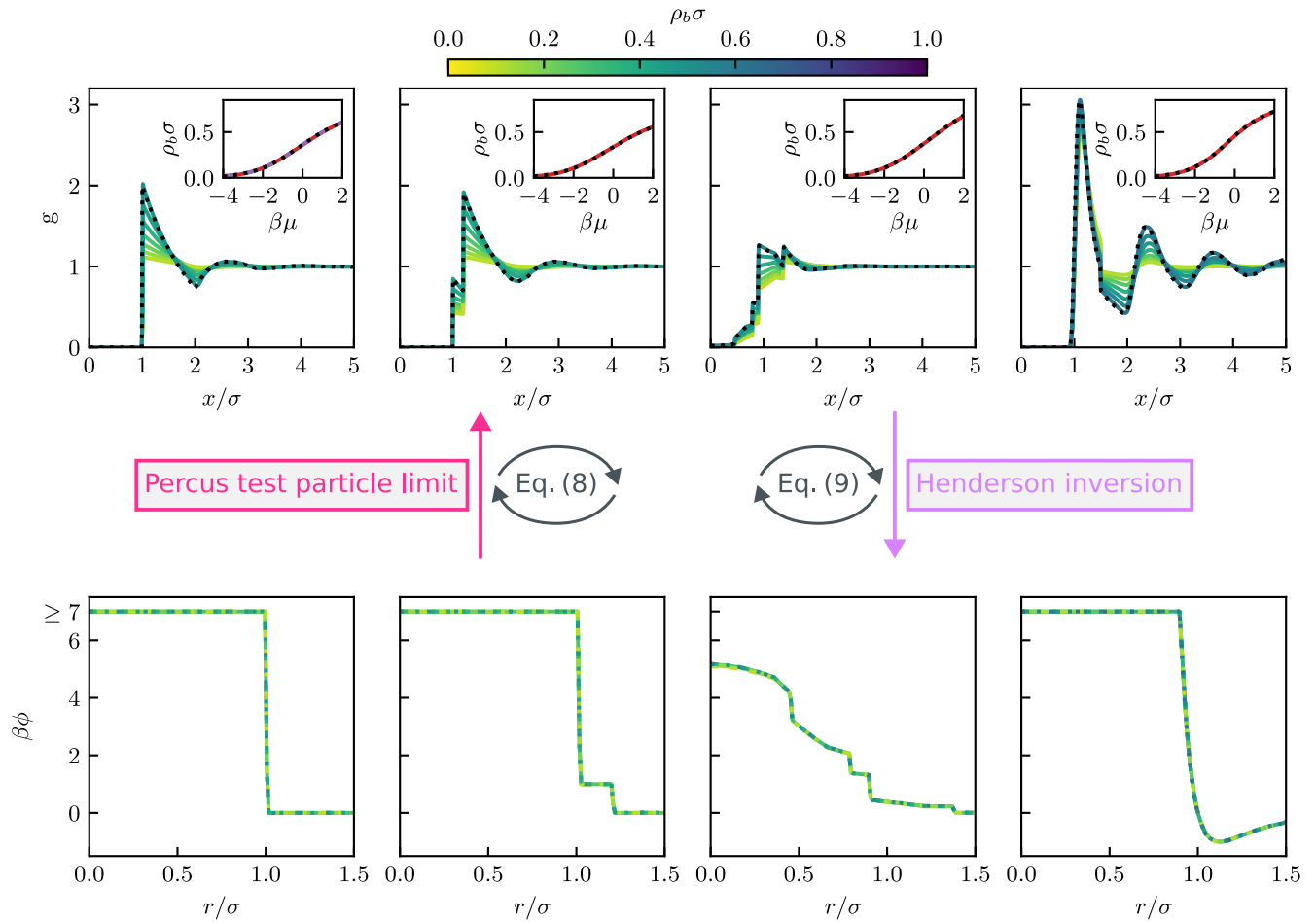


FIG. 2. Pair structure and Henderson design via the neural metadensity functional. Results are shown for the pair distribution function $g(r)$ (first row) and corresponding scaled pair potential $\beta\phi(r)$ (second row) for different values of scaled bulk density $\rho_b\sigma$ (color bar) and for four different pair potentials $\beta\phi(r)$ in one dimension: (i) hard rods (first column), (ii) square-shoulder repulsion (second column), (iii) random penetrable repulsion (third column), and (iv) LJ particles (fourth column). Results for $g(r)$ from test particle minimization (8) with $\beta\phi(r)$ fixed and $\beta\mu = -2, -1.5, 1, -0.5, 0.5, 1$ (yellow to green lines) are numerically identical to the simulation reference (black dots, shown for $\beta\mu = 1$). The variable r denotes one-dimensional relative distance. Insets: the neural equations of state $\rho_b\sigma$ versus $\beta\mu$ (red lines) agree with reference simulation data (black dots) and for hard rods with the exact solution (dashed violet line, first panel); we set the de Broglie wavelength $\Lambda = \sigma$ in the ideal gas contribution. Using solely $g(r), \rho_b, \beta$ as input, Henderson density functional inversion (9) allows one to reconstruct $\beta\phi(r)$ consistently (overlapping dashed colored lines) and with high accuracy across the entire range of densities considered (color bar); we take values $\beta\phi(r) \geq 7$ to represent numerically hard cores.

in the form $c_1(\mathbf{r}, [\rho, \beta\phi]) - \ln \rho(\mathbf{r}) - \beta V_{\text{ext}}(\mathbf{r}) + \beta\mu = 0$. The required “slope” is the metadirect correlation functional obtained by automatic differentiation keeping $\rho(\mathbf{r})$ fixed: $c_\phi(\mathbf{r}, r'; [\rho, \beta\phi]) = \delta c_1(\mathbf{r}; [\rho, \beta\phi]) / \delta \beta\phi(r')$; see Appendix B for its relevance in analyzing fluctuations via the meta-Ornstein-Zernike route. The results for $\beta\phi(r)$ in Fig. 3 demonstrate that the true pair potential can be reconstructed reliably. Some weak noise is visible in the four $\beta\phi(r)$. Such artifacts tend to increase for more extreme cases of $\beta\phi(r)$. Overall, the quality of the results is remarkable.

While Henderson’s uniqueness theorem is formulated canonically [31,42], here we worked in the grand ensemble

and provided a corresponding proof in Appendix C. Using the neural metafunctional, we validated uniqueness in test particle situations (Fig. 2). We also found empirically unique solutions in a much wider class of inhomogeneous systems: The hard-wall pore (Fig. 3) is a representative example. Future work should address this generalized inversion problem formally. Regarding higher-dimensional systems, when working with planar symmetry and randomizing the external potential $\beta V_{\text{ext}}(x)$ [21–28] as well as $\beta\phi(r)$ to generate training data, our setup remains applicable. Henderson inversion is then formally guaranteed via conversion from planar to radial symmetry [18,21,26,27].

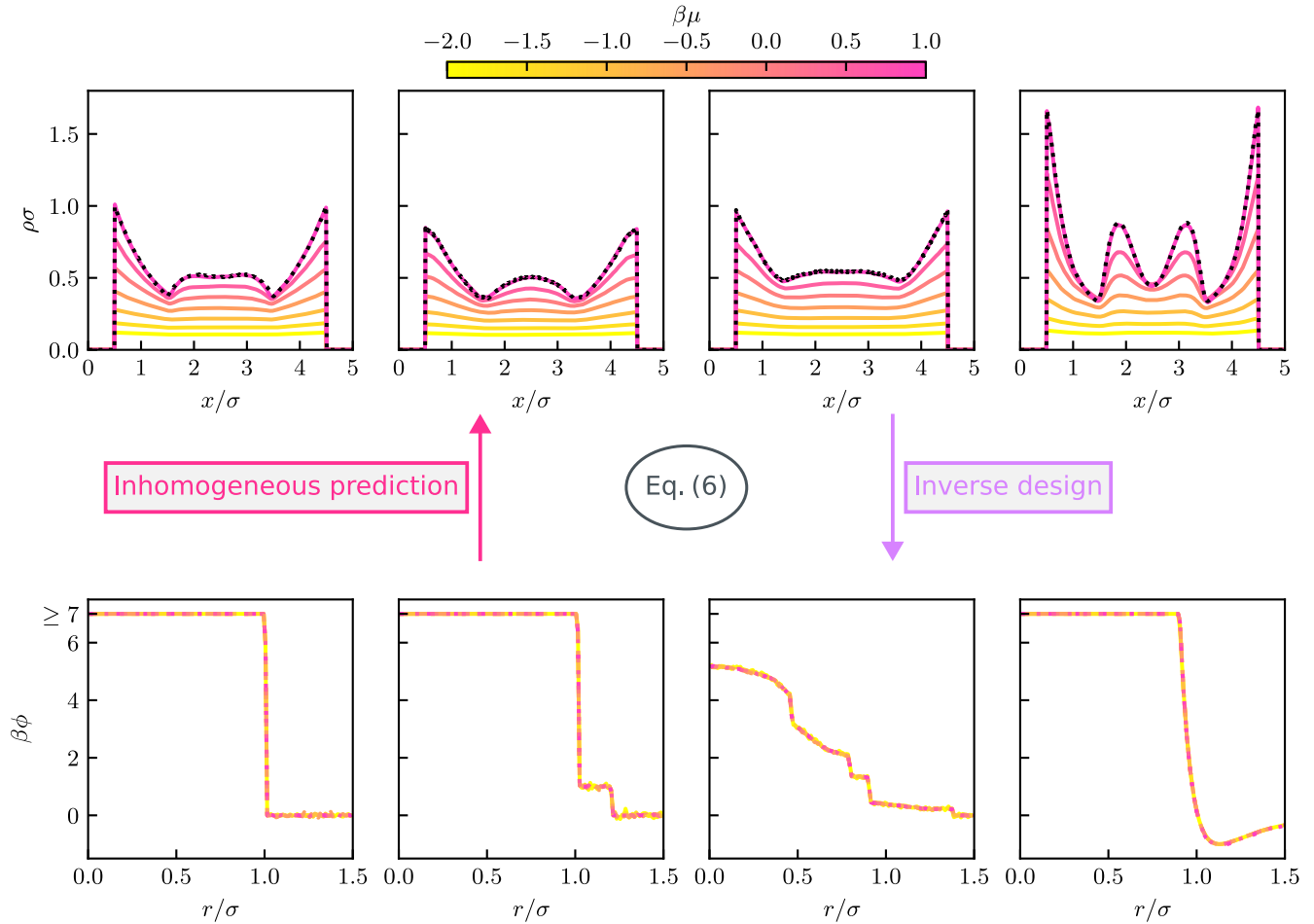


FIG. 3. Metadensity functional application for confinement between two hard walls located at $x/\sigma = 0.5$ and 4.5 at varying values of the scaled chemical potential $\beta\mu$ (color bar). Results are shown for scaled one-body density profiles $\rho(x)\sigma$ (first row, lines) from density functional minimization (6) for each of the four representative pair potentials $\beta\phi(r)$ of Fig. 2 fixed (second row). Simulation results (black dotted lines) are shown for $\beta\mu = 1$. Setting the density profile $\rho(x)$ as the target and keeping the hard walls unchanged, inhomogeneous inverse pair potential design aims to find the corresponding, as-yet unknown, pair potential $\beta\phi(r)$, where r indicates one-dimensional distance. For each system, the results for $\beta\phi(r)$ (second row), obtained from Eq. (6) for each of the seven values of $\beta\mu$ separately, coincide numerically with each other as well as with the reference, up to very small artifacts (overlapping dashed colored lines). This demonstrates successful pair potential reconstruction and inverse design.

Instead of the test particle route to $g(r)$, one could use the Ornstein-Zernike equation together with the neural bulk pair direct correlation function [18,21,26–28]. It would also be interesting to relate to exact solutions for bulk one-dimensional systems [55,57–59], test particle sum rules [60], quantum test particle concepts [61], liquid integral equation theory [62,63], entropy functionals [64,65], data-driven approaches [66], differentiable simulations [67], experimental work [68–70], splitting of interparticle interactions [28,71,72], and self-assembly [73].

Acknowledgments—We thank Josh Robinson and Sophie Hermann for helpful discussions. R. E. acknowledges support of the Leverhulme Trust Grant No. EM-2020-029/4.

This work is supported by the Deutsche Forschungsgemeinschaft under Project No. 551294732.

Data availability—The data that support the findings of this Letter are openly available [51].

- [1] R. Evans, The nature of the liquid-vapour interface and other topics in the statistical mechanics of non-uniform, classical fluids, *Adv. Phys.* **28**, 143 (1979).
- [2] R. Evans, Density functionals in the theory of nonuniform fluids, Chap. 3 in *Fundamentals of Inhomogeneous Fluids*, edited by D. Henderson (Dekker, New York, 1992).
- [3] J. P. Hansen and I. R. McDonald, *Theory of Simple Liquids*, 4th ed. (Academic Press, London, 2013).

- [4] R. Evans, M. Oettel, R. Roth, and G. Kahl, New developments in classical density functional theory, *J. Phys. Condens. Matter* **28**, 240401 (2016).
- [5] M. Schmidt, Power functional theory for many-body dynamics, *Rev. Mod. Phys.* **94**, 015007 (2022).
- [6] Y. Rosenfeld, Scaled field particle theory of the structure and the thermodynamics of isotropic hard particle fluids, *J. Chem. Phys.* **89**, 4272 (1988).
- [7] Y. Rosenfeld, Free-energy model for the inhomogeneous hard-sphere fluid mixture and density-functional theory of freezing, *Phys. Rev. Lett.* **63**, 980 (1989).
- [8] P. Tarazona, Density functional for hard sphere crystals: A fundamental measure approach, *Phys. Rev. Lett.* **84**, 694 (2000).
- [9] R. Roth, Fundamental measure theory for hard-sphere mixtures: A review, *J. Phys. Condens. Matter* **22**, 063102 (2010).
- [10] T. Santos-Silva, P. I. C. Teixeira, C. Anquetil-Deck, and D. J. Cleaver, Neural-network approach to modeling liquid crystals in complex confinement, *Phys. Rev. E* **89**, 053316 (2014).
- [11] S.-C. Lin and M. Oettel, A classical density functional from machine learning and a convolutional neural network, *SciPost Phys.* **6**, 025 (2019).
- [12] S.-C. Lin, G. Martius, and M. Oettel, Analytical classical density functionals from an equation learning network, *J. Chem. Phys.* **152**, 021102 (2020).
- [13] P. Cats, S. Kuipers, S. de Wind, R. van Damme, G. M. Coli, M. Dijkstra, and R. van Roij, Machine-learning free-energy functionals using density profiles from simulations, *APL Mater.* **9**, 031109 (2021).
- [14] C. Qiao, X. Yu, X. Song, T. Zhao, X. Xu, S. Zhao, and K. E. Gubbins, Enhancing gas solubility in nanopores: A combined study using classical density functional theory and machine learning, *Langmuir* **36**, 8527 (2020).
- [15] P. Yatsyshin, S. Kalliadasis, and A. B. Duncan, Physics-constrained Bayesian inference of state functions in classical density-functional theory, *J. Chem. Phys.* **156**, 074105 (2022).
- [16] A. Malpica-Morales, P. Yatsyshin, M. A. Duran-Olivencia, and S. Kalliadasis, Physics-informed Bayesian inference of external potentials in classical density functional theory, *J. Chem. Phys.* **159**, 104109 (2023).
- [17] X. Fang, M. Gu, and J. Wu, Reliable emulation of complex functionals by active learning with error control, *J. Chem. Phys.* **157**, 214109 (2022).
- [18] J. Dijkman, M. Dijkstra, R. van Roij, M. Welling, J.-W. van de Meent, and B. Ensing, Learning neural free-energy functionals with pair-correlation matching, *Phys. Rev. Lett.* **134**, 056103 (2025).
- [19] M. M. Kelley, J. Quinton, K. Fazel, N. Karimitari, C. Sutton, and R. Sundararaman, Bridging electronic and classical density-functional theory using universal machine-learned functional approximations, *J. Chem. Phys.* **161**, 144101 (2024).
- [20] D. de las Heras, T. Zimmermann, F. Sammüller, S. Hermann, and M. Schmidt, Perspective: How to overcome dynamical density functional theory, *J. Phys. Condens. Matter* **35**, 271501 (2023).
- [21] F. Sammüller, S. Hermann, D. de las Heras, and M. Schmidt, Neural functional theory for inhomogeneous fluids: Fundamentals and applications, *Proc. Natl. Acad. Sci. U.S.A.* **120**, e2312484120 (2023).
- [22] F. Sammüller, S. Hermann, and M. Schmidt, Why neural functionals suit statistical mechanics, *J. Phys. Condens. Matter* **36**, 243002 (2024).
- [23] F. Sammüller, Neural functional theory for inhomogeneous fluids—Tutorial; for online access see <https://github.com/sfalmo/NeuralDFT-Tutorial>.
- [24] F. Sammüller, S. Robitschko, S. Hermann, and M. Schmidt, Hyperdensity functional theory of soft matter, *Phys. Rev. Lett.* **133**, 098201 (2024).
- [25] F. Sammüller and M. Schmidt, Why hyperdensity functionals describe any equilibrium observable, *J. Phys. Condens. Matter* **37**, 083001 (2025).
- [26] F. Sammüller and M. Schmidt, Neural density functionals: Local learning and pair-correlation matching, *Phys. Rev. E* **110**, L032601 (2024).
- [27] F. Sammüller, M. Schmidt, and R. Evans, Neural density functional theory of liquid-gas phase coexistence, *Phys. Rev. X* **15**, 011013 (2025).
- [28] A. T. Bui and S. J. Cox, Learning classical density functionals for ionic fluids, [arXiv:2410.02556](https://arxiv.org/abs/2410.02556).
- [29] A. G. Baydin, B. A. Pearlmutter, A. A. Radul, and J. M. Siskind, Automatic differentiation in machine learning: A survey, *J. Mach. Learn. Res.* **18**, 1 (2018), <http://jmlr.org/papers/v18/17-468.html>.
- [30] R. Stierle, G. Bauer, N. Thiele, B. Bursik, P. Rehner, and J. Gross, Classical density functional theory in three dimensions with GPU-accelerated automatic differentiation: Computational performance analysis using the example of adsorption in covalent-organic frameworks, *Chem. Eng. Sci.* **298**, 120380 (2024).
- [31] R. L. Henderson, A uniqueness theorem for fluid pair correlation functions, *Phys. Lett.* **49A**, 197 (1974).
- [32] M. D. Johnson, P. Hutchinson, and N. H. March, Ion-ion oscillatory potentials in liquid metals *Proc. R. Soc. A* **282**, 283 (1964).
- [33] D. Levesque, J. J. Weis, and L. Reatto, Pair interaction from structural data for dense classical liquids, *Phys. Rev. Lett.* **54**, 451 (1985).
- [34] J. E. Enderby, The influence of interatomic forces on the structure of liquids: An experimental approach, *Philos. Mag. A* **58**, 5 (1988).
- [35] R. Evans, Comment on reverse Monte Carlo simulation, *Mol. Simul.* **4**, 409 (1990).
- [36] J. K. Percus, Some solvable models of nonuniform classical fluids, *J. Stat. Phys.* **42**, 921 (1986).
- [37] R. L. McGreevy, Reverse Monte Carlo modelling, *J. Phys. Condens. Matter* **13**, R877 (2001).
- [38] F. Frommer, M. Hanke, and S. Jansen, A note on the uniqueness result for the inverse Henderson problem, *J. Math. Phys. (N.Y.)* **60**, 093303 (2019).
- [39] F. Frommer and M. Hanke, A variational framework for the inverse Henderson problem of statistical mechanics, *Lett. Math. Phys.* **112**, 71 (2022).
- [40] A. Moradzadeh and N. R. Aluru, Understanding simple liquids through statistical and deep learning approaches, *J. Chem. Phys.* **154**, 204503 (2021).

- [41] G. Tóth, N. Király, and A. Vrabcz, Pair potentials from diffraction data on liquids: A neural network solution, *J. Chem. Phys.* **123**, 174109 (2005).
- [42] H. Wang, F.H. Stillinger, and S. Torquato, Sensitivity of pair statistics on pair potentials in many-body systems, *J. Chem. Phys.* **153**, 124106 (2020).
- [43] S. Torquato and H. Wang, Precise determination of pair interactions from pair statistics of many-body systems in and out of equilibrium, *Phys. Rev. E* **106**, 044122 (2022).
- [44] R. B. Jadrich, J. A. Bollinger, B. A. Lindquist, and T. M. Truskett, Equilibrium cluster fluids: Pair interactions via inverse design, *Soft Matter* **11**, 9342 (2015).
- [45] H. Wang and S. Torquato, Designer pair statistics of disordered many-particle systems with novel properties, *J. Chem. Phys.* **160**, 044911 (2024).
- [46] J. C. Dyre, Simple liquids' quasiuniversality and the hard-sphere paradigm, *J. Phys. Condens. Matter* **28**, 323001 (2016).
- [47] A. E. Stones, R. P. A. Dullens, and D. G. A. L. Aarts, Model-free measurement of the pair potential in colloidal fluids using optical microscopy, *Phys. Rev. Lett.* **123**, 098002 (2019).
- [48] M. Levy, Universal variational functionals of electron densities, first-order density matrices, and natural spin-orbitals and solution of the v-representability problem, *Proc. Natl. Acad. Sci. U.S.A.* **76**, 6062 (1979).
- [49] W. S. B. Dwandaru and M. Schmidt, Variational principle of classical density functional theory via Levy's constrained search method, *Phys. Rev. E* **83**, 061133 (2011).
- [50] N. D. Mermin, Thermal properties of the inhomogeneous electron gas, *Phys. Rev.* **137**, A1441 (1965).
- [51] Code, simulation data, and neural functionals available at: <https://github.com/S-K-acc/metafunctional>.
- [52] J. K. Percus, Approximation methods in classical statistical mechanics, *Phys. Rev. Lett.* **8**, 462 (1962).
- [53] J. K. Percus, Equilibrium state of a classical fluid of hard rods in an external field, *J. Stat. Phys.* **15**, 505 (1976).
- [54] A. Robledo and C. Varea, On the relationship between the density functional formalism and the potential distribution theory for nonuniform fluids, *J. Stat. Phys.* **26**, 513 (1981).
- [55] A. M. Montero and A. Santos, Triangle-well and ramp interactions in one-dimensional fluids: A fully analytic exact solution, *J. Stat. Phys.* **175**, 269 (2019).
- [56] L. Tonks, The complete equation of state of one-, two- and three-dimensional gases of hard elastic spheres, *Phys. Rev.* **50**, 955 (1936).
- [57] A. J. Archer and R. Evans, Relationship between local molecular field theory and density functional theory for nonuniform liquids, *J. Chem. Phys.* **138**, 014502 (2013).
- [58] A. J. Archer, B. Chacko, and R. Evans, The standard mean-field treatment of inter-particle attraction in classical DFT is better than one might expect, *J. Chem. Phys.* **147**, 034501 (2017).
- [59] A. M. Montero, A. Rodriguez-Rivas, S. B. Yustea, A. Santosa, and M. Lopez de Haro, On a conjecture concerning the Fisher-Widom line and the line of vanishing excess isothermal compressibility in simple fluids, *Mol. Phys.* **122**, e2357270 (2024).
- [60] M. Gül, R. Roth, and R. Evans, Using test particle sum rules to construct accurate functionals in classical density functional theory, *Phys. Rev. E* **110**, 064115 (2024).
- [61] R. J. McCarty, D. Perchak, R. Pederson, R. Evans, Y. Qiu, S. R. White, and K. Burke, Bypassing the energy functional in density functional theory: Direct calculation of electronic energies from conditional probability densities, *Phys. Rev. Lett.* **125**, 266401 (2020).
- [62] I. Pihlajamaa and L. M. C. Janssen, Comparison of integral equation theories of the liquid state, *Phys. Rev. E* **110**, 044608 (2024).
- [63] R. E. A. Goodall and A. A. Lee, Data-driven approximations to the bridge function yield improved closures for the Ornstein-Zernike equation, *Soft Matter* **17**, 5393 (2021).
- [64] J. K. Percus, The structure of density functionals, *J. Phys. Condens. Matter* **6**, A125 (1994).
- [65] D. M. Nicholson, C. Y. Gao, M. T. McDonnell, C. C. Sluss, and David J. Keffer, Entropy pair functional theory: Direct entropy evaluation spanning phase transitions, *Entropy* **23**, 234 (2021).
- [66] M.-C. Chang, C.-H. Tung, S.-Y. Chang, J. M. Carrillo, Y. Wang, B. G. Sumpter, G.-R. Huang, C. Do, and W.-R. Chen, A machine learning inversion scheme for determining interaction from scattering, *Commun. Phys.* **5**, 46 (2022).
- [67] W. Wang, Z. Wu, J. C. B. Dietschreit, and R. Gómez-Bombarelli, Learning pair potentials using differentiable simulations, *J. Chem. Phys.* **158**, 044113 (2023).
- [68] M. C. R. Bell-Davies, J. Codina, A. Curran, J. Dobnikar, R. P. A. Dullens, and I. Pagonabarraga, Direct measurement of repulsive and attractive pair potentials using pairs of optical traps, *J. Chem. Phys.* **160**, 184201 (2024).
- [69] A. E. Stones, R. P. A. Dullens, and D. G. A. L. Aarts, Communication: Contact values of pair distribution functions in colloidal hard disks by test-particle insertion, *J. Chem. Phys.* **148**, 241102 (2018).
- [70] A. E. Stones and D. G. A. L. Aarts, Measuring many-body distribution functions in fluids using test-particle insertion, *J. Chem. Phys.* **159**, 194502 (2023).
- [71] S. J. Cox, Dielectric response with short-ranged electrostatics, *Proc. Natl. Acad. Sci. U.S.A.* **117**, 19746 (2020).
- [72] A. T. Bui and S. J. Cox, A classical density functional theory for solvation across length scales, *J. Chem. Phys.* **161**, 104103 (2024).
- [73] M. Wassermair, G. Kahl, R. Roth, and A. J. Archer, Fingerprints of ordered self-assembled structures in the liquid phase of a hard-core, square-shoulder system, *J. Chem. Phys.* **161**, 124503 (2024).
- [74] R. Evans and M. C. Stewart, The local compressibility of liquids near non-adsorbing substrates: A useful measure of solvophobicity and hydrophobicity?, *J. Phys. Condens. Matter* **27**, 194111 (2015).
- [75] R. Evans, M. C. Stewart, and N. B. Wilding, A unified description of hydrophilic and superhydrophobic surfaces in terms of the wetting and drying transitions of liquids, *Proc. Natl. Acad. Sci. U.S.A.* **116**, 23901 (2019).
- [76] M. K. Coe, R. Evans, and N. B. Wilding, Density depletion and enhanced fluctuations in water near hydrophobic

solutes: Identifying the underlying physics, *Phys. Rev. Lett.* **128**, 045501 (2022).

[77] T. Eckert, N. C. X. Stuhlmüller, F. Sammüller, and M. Schmidt, Fluctuation profiles in inhomogeneous fluids, *Phys. Rev. Lett.* **125**, 268004 (2020).

[78] T. Eckert, N. C. X. Stuhlmüller, F. Sammüller, and M. Schmidt, Local measures of fluctuations in inhomogeneous liquids: Statistical mechanics and illustrative applications, *J. Phys. Condens. Matter* **35**, 425102 (2023).

End Matter

Appendix A: Parametric metadensity functional—Instead of machine learning the functional dependence on $\beta\phi(r)$ on a discretized grid, one can work with parametric dependence on the pair interaction parameters. Although this restricts the general applicability of the resulting neural metafunctional, it can be more efficient within the range of applicability. We

demonstrate the method for square-shoulder pair potentials with scaled shoulder range Δ/σ and height $\beta\epsilon$, where both parameters are used as input nodes, similar to thermal training [27]. Results from inhomogeneous and test particle DFT of the parametrized metadensity functional $c_1(\mathbf{r}; [\rho], \beta\epsilon, \Delta/\sigma)$ shown in Fig. 4 demonstrate high accuracy. We expect the parametrization method to apply to many-body interparticle interaction potentials $u(\mathbf{r}_1, \dots, \mathbf{r}_N; \alpha_1, \dots, \alpha_m)$ via machine learning the dependence on m interaction parameters $\alpha_1, \dots, \alpha_m$ to provide parametrized access to $c_1(\mathbf{r}; [\rho, \beta u]) = c_1(\mathbf{r}; [\rho], \beta, \alpha_1, \dots, \alpha_m)$.

Appendix B: Fluctuations—We address the fluctuation structure by functionally differentiating the (logarithm of the) Euler-Lagrange equation (6) with respect to $\beta\phi(r')$ keeping μ , β , and $V_{\text{ext}}(\mathbf{r})$ fixed. Rearranging the result yields the following exact meta-Ornstein-Zernike (OZ) equation:

$$c_\phi(\mathbf{r}, \mathbf{r}'; [\rho, \beta\phi]) = \frac{\chi_\phi(\mathbf{r}, \mathbf{r}')}{\rho(\mathbf{r})} - \int d\mathbf{r}'' c_2(\mathbf{r}, \mathbf{r}''; [\rho, \beta\phi]) \chi_\phi(\mathbf{r}'', \mathbf{r}'), \quad (\text{B1})$$

where $c_2(\mathbf{r}, \mathbf{r}'; [\rho, \beta\phi]) = \delta c_1(\mathbf{r}; [\rho, \beta\phi]) / \delta \rho(\mathbf{r}')$ [1–3] and the local metacompressibility is $\chi_\phi(\mathbf{r}, \mathbf{r}') = \delta \rho(\mathbf{r}) / \delta \beta\phi(\mathbf{r}')|_{\beta(V_{\text{ext}} - \mu)}$, generalizing the local compressibility $\chi_\mu(\mathbf{r})$ [74–76] and its extensions [24,25,77,78]. Equation (B1) mirrors closely the inhomogeneous two-body [1–5], nonequilibrium [5], fluctuation [77,78], and hyperdensity [24,25] OZ relations. Figure 5 shows representative results for $\chi_\phi(\mathbf{r}, \mathbf{r}')$ and $c_\phi(\mathbf{r}, \mathbf{r}')$ for the LJ system. The highly structured behavior in both functions reflects the oscillations in the density profile.

One can readily show that the local metacompressibility constitutes the following average: $\chi_\phi(\mathbf{r}', r) = -\text{cov}[\hat{\rho}(\mathbf{r}'), \hat{G}(r)]$, where the density “operator” is $\hat{\rho}(\mathbf{r}) = \sum_i \delta(\mathbf{r} - \mathbf{r}_i)$, and we have defined a global measure of mutual particle distances $\hat{G}(r) = \frac{1}{2} \sum'_{ij} \delta(r - |\mathbf{r}_i - \mathbf{r}_j|)$, where the primed double sum is over distinct pairs $i \neq j$. Then, Eq. (B1) can be viewed as a special case of the hyper-OZ relation [24,25] for the observable $\hat{A} = -\hat{G}(r)$.

The test particle situation requires functionally differentiating the corresponding Euler-Lagrange equation (8)

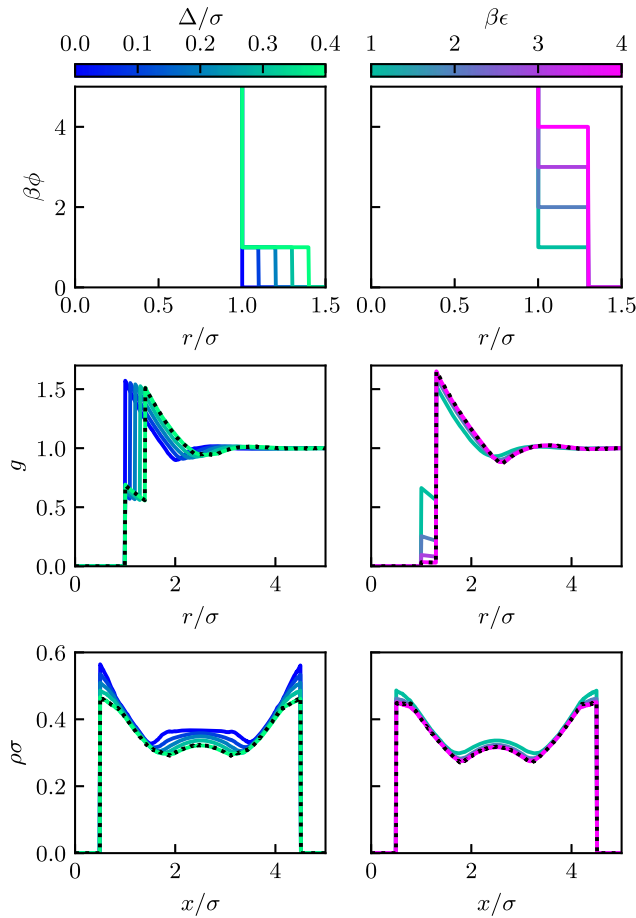


FIG. 4. Parametric metadensity functional applications. The scaled range (Δ/σ) and depth ($\beta\epsilon$) parameters of the square-shoulder potential are treated as neural network input nodes that control the form of $\beta\phi(r)$ (first row). Percus test particle minimization (8) yields results for $g(r)$ (second row) for the fluids described by the different $\phi(r)$ for $\beta\mu = 0$. Inhomogeneous density functional minimization (6) yields corresponding results for $\rho(x)\sigma$ under confinement between two hard walls at $x/\sigma = 0.5$ and 4.5 (third row). Representative simulation results (dotted lines) are shown for the largest values of Δ/σ and $\beta\epsilon$ considered.

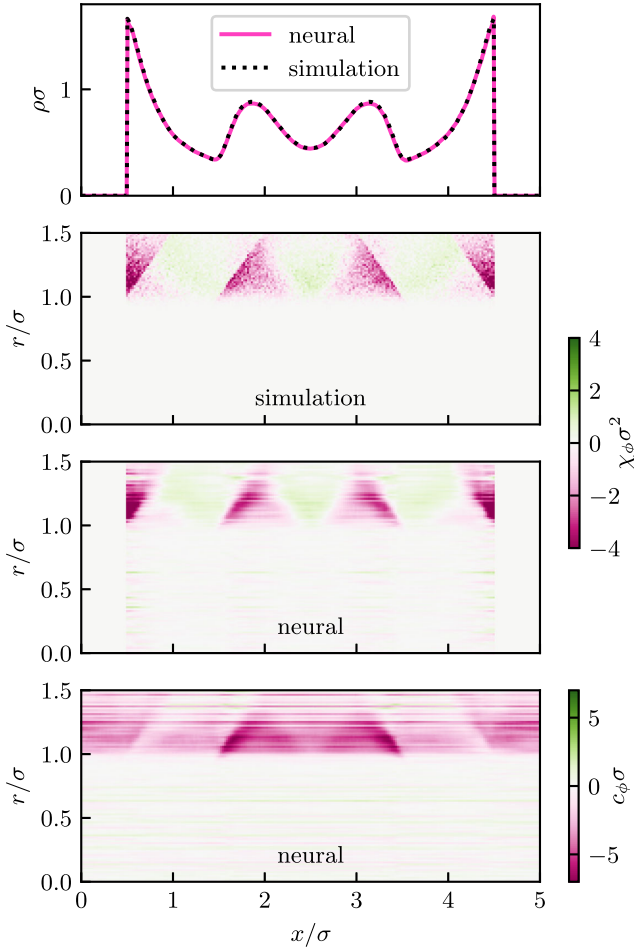


FIG. 5. Meta-OZ results. The density profile for $\beta\mu = 1$ for the truncated LJ system, with $r_c = 1.5\sigma$, in hard-wall confinement is shown (first panel). Corresponding results are shown as a function of the scaled position x/σ and interparticle distance r/σ , for the local metacompressibility $\chi_\phi(x, r)$ from simulations (second panel) and from the neural functional (third panel), and for the metadirect correlation function $c_\phi(x, r)$ (fourth panel).

with respect to $\beta\phi(r')$, yielding the test particle meta-OZ relation:

$$c_\phi(r, r'; [\rho_g, \beta\phi]) - \delta(r - r') = \frac{\chi_g(r, r')}{\rho_g(r)} - \int d\mathbf{r}'' c_2(\mathbf{r}, \mathbf{r}''; [\rho_g, \beta\phi]) \chi_g(|\mathbf{r}''|, r'), \quad (\text{B2})$$

where $\rho_g(r) = \rho_b g(r)$ and the scaled bulk pair metacompressibility is $\beta\chi_g(r, r') = \delta\rho_g(r)/\delta\phi(r')$, which is closely related to $\delta g(r)/\delta\phi(r')$, as identified and highlighted as important by Wang *et al.* in their introduction [42].

Appendix C: Functional relationships—As is pertinent to the treatment in the main text, we give a grand canonical version of Henderson’s theorem. The equilibrium probability density is given by $f_0 = e^{-\beta(H-\mu N)}/\Xi$, where the Hamiltonian $H = K + \Phi + \mathcal{V}_{\text{ext}}$, with kinetic energy

$K = \sum_{i=1}^N \mathbf{p}_i^2/(2m)$, interparticle potential energy $\Phi = \sum_{i \neq j} \phi(\mathbf{r}_i - \mathbf{r}_j)/2$, and external potential energy $\mathcal{V}_{\text{ext}} = \sum_{i=1}^N V_{\text{ext}}(\mathbf{r}_i)$. We keep only the pair potential $\phi(r)$. Wang *et al.* [42] generalize Φ to include higher-body potentials but work in the canonical ensemble. Following Appendix B in Ref. [3], we introduce the functional

$$\Omega[f] = \text{Tr} f(H - \mu N + \beta^{-1} \ln f). \quad (\text{C1})$$

In equilibrium: $\Omega[f_0] = -\beta^{-1} \ln \Xi$, where $\Xi = \text{Tr} e^{-\beta(H-\mu N)}$ is the grand partition function, and therefore, $\Omega[f_0] = \Omega$ is the grand potential. One can prove

$$\Omega[f] \geq \Omega[f_0] \quad (\text{C2})$$

using a Gibbs-Bogoliubov inequality.

To derive Henderson’s theorem, consider two different Hamiltonians—the original H and $H' = K + \Phi' + \mathcal{V}'$. Now Φ' is a sum of pair potentials ϕ' , and $\mathcal{V}'_{\text{ext}}$ corresponds to the external potential $V'_{\text{ext}}(\mathbf{r})$. The chemical potential μ' might also be different. Associated with H' is the equilibrium f'_0 and Ω'_0 .

Equation (C2) asserts $\Omega' = \text{Tr} f'_0(H' - \mu' N + \beta^{-1} \ln f'_0) \leq \text{Tr} f_0(H' - \mu' N + \beta^{-1} \ln f_0)$. The right-hand side is $\text{Tr} f_0(H - \mu N + \Phi' - \Phi + \mathcal{V}'_{\text{ext}} - \mathcal{V}_{\text{ext}} + \mu N - \mu' N + \beta^{-1} \ln f_0)$. Thus,

$$\Omega' \leq \Omega[f_0] + \text{Tr} f_0[\Phi' - \Phi + (\mathcal{V}'_{\text{ext}} - \mu' N) - (\mathcal{V}_{\text{ext}} - \mu N)]. \quad (\text{C3})$$

Note that $\mathcal{V}_{\text{ext}} - \mu N = \sum_{i=1}^N (V_{\text{ext}}(\mathbf{r}_i) - \mu) = -\int d\mathbf{r} \hat{\rho}(\mathbf{r}) \psi(\mathbf{r})$ with “intrinsic” chemical potential $\psi(\mathbf{r}) = \mu - V_{\text{ext}}(\mathbf{r})$. Then, Eq. (C3) reads

$$\Omega' \leq \Omega + \text{Tr} f_0(\Phi' - \Phi) - \int d\mathbf{r} \rho(\mathbf{r}) [\psi'(\mathbf{r}) - \psi(\mathbf{r})]. \quad (\text{C4})$$

Swapping primed and unprimed variables, i.e., using H and f_0 , one finds

$$\Omega \leq \Omega' + \text{Tr} f'_0(\Phi - \Phi') - \int d\mathbf{r} \rho'(\mathbf{r}) [\psi(\mathbf{r}) - \psi'(\mathbf{r})], \quad (\text{C5})$$

where $\rho(\mathbf{r})$ is the equilibrium one-body density corresponding to f_0 and $\rho'(\mathbf{r})$ that for f'_0 . (i) Suppose the pair potentials are identical: $\phi'(r) = \phi(r)$; i.e., we are considering identical fluids in a reservoir at given $\mu' = \mu$, but exposed to different external potentials $V'_{\text{ext}}(\mathbf{r})$ and $V_{\text{ext}}(\mathbf{r})$.

What occurs if one requires $\rho'(\mathbf{r}) = \rho(\mathbf{r})$? Adding Eqs. (C4) and (C5):

$$\Omega' + \Omega \leq \Omega + \Omega', \quad (\text{C6})$$

a clear contradiction as equality holds only in the trivial case of the primed and unprimed systems being identical; i.e., there is a unique $V_{\text{ext}}(\mathbf{r})$ [or $\psi(\mathbf{r})$] that gives rise to a given $\rho(\mathbf{r})$, a key result in the foundation of DFT [1,3,50]. (ii) Suppose now $\psi'(\mathbf{r}) = \psi(\mathbf{r})$; i.e., the intrinsic chemical potentials are identical, but the pair potentials can be different. The final terms in Eqs. (C4) and (C5) vanish, and one can write Eqs. (C4) and (C5), respectively, as

$$\Omega' \leq \Omega + \frac{1}{2} \int d\mathbf{r}_1 d\mathbf{r}_2 \rho^{(2)}(\mathbf{r}_1, \mathbf{r}_2) [\phi'(\mathbf{r}_{12}) - \phi(\mathbf{r}_{12})], \quad (\text{C7})$$

$$\Omega \leq \Omega' + \frac{1}{2} \int d\mathbf{r}_1 d\mathbf{r}_2 \rho^{(2)'}(\mathbf{r}_1, \mathbf{r}_2) [\phi(\mathbf{r}_{12}) - \phi'(\mathbf{r}_{12})], \quad (\text{C8})$$

where $\mathbf{r}_{12} = \mathbf{r}_1 - \mathbf{r}_2$ and $\rho^{(2)}(\mathbf{r}_1, \mathbf{r}_2)$ is the two-body distribution function corresponding to f_0 and $\rho^{(2)'}(\mathbf{r}_1, \mathbf{r}_2)$ that for f'_0 . Suppose now $\rho^{(2)}(\mathbf{r}_1, \mathbf{r}_2) = \rho^{(2)'}(\mathbf{r}_1, \mathbf{r}_2)$, then adding Eqs. (C7) and (C8) one finds again Eq. (C6). The contradiction implies that there is a unique $\phi(r)$ that gives rise to a given $\rho^{(2)}(\mathbf{r}_1, \mathbf{r}_2)$.

This argument is equivalent to that of Henderson [31] who worked in the canonical ensemble; see his Eqs. (4) and (5). For the uniform fluid $\rho^{(2)}(\mathbf{r}_1, \mathbf{r}_2) = \rho_b^2 g(r_{12}; \rho_b)$ where ρ_b is the uniform density at specified μ , T , and $g(r_{12}; \rho_b)$ is the radial distribution function. It follows that the latter determines uniquely $\phi(r)$.